Deciphering the Molecular Details of the Lipoxin Formation Mechanism in the 5(*S*),15(*S*)-diHpETE Biosynthetic Pathway Catalyzed by Reticulocyte 15-Lipoxygenase-1.

Alejandro Cruz[1], Àngels González-Lafont[1, 2] and José M. Lluch[1, 2 *]

[1] Departament de Química and [2] Institut de Biotecnologia i de Biomedicina (IBB), Universitat Autònoma de Barcelona, 08193 Bellaterra, Barcelona Spain

Email: JoseMaria.Lluch@uab.cat

Abstract

Chronic inflammation is now widely recognized to play important roles in many commonly occurring diseases, including COVID-19. The resolution response to this chronic inflammation is an active process governed by specialized pro-resolving mediators (SPMs) like the lipid mediators known as lipoxins. The biosynthesis of lipoxins is catalyzed from arachidonic acid by several lipoxygenases. However, the molecular details of the mechanisms involved are not well known yet. In this paper, we have combined molecular dynamics (MD) simulations and quantum mechanics/molecular mechanics (QM/MM) calculations to analyze how reticulocyte 15-LOX-1 catalyzes the production of lipoxins from 5(*S*),15(*S*)-diHpETE. Our results indicate that the dehydration mechanism from 5(*S*),15(*S*)-diHpETE, via the formation of an epoxide, presents huge energy barriers even though it was one of the two *a priori* synthetic proposals. This result is compatible with the fact that no epoxide has been directly detected as an intermediate in the catalytic formation of lipoxins from 5(*S*),15(*S*)-diHpETE. Conversely, the oxygenation at C_{14} of 5(*S*),15(*S*)-diHpETE is feasible because

there is an open channel connecting the protein surface with this carbon atom, and the energy barrier for oxygen addition through this channel is small. The analysis of the following steps of this mechanism, leading to the corresponding hydroperoxide at the 15-LOX-1 active site, indicates that the oxygenation mechanism will lead to the formation of lipoxinB_4 after the final action of a reductase. In contrast, our calculations indicate in agreement with experiments that lipoxinA_4 cannot derive from 5(*S*),15(*S*)-diHpETE by either of the two proposed mechanisms, and that 5(*S*),15(*S*)-diHETE is not an intermediate of lipoxin biosynthesis catalyzed by 15-LOX-1.

Keywords

Lipoxins; Biosynthetic pathways; 15-Lipoxygenase; Hydrogen abstraction reactions; Dehydration mechanism; Oxygen access channels; QM/MM calculations; Molecular dynamics simulations.

1. Introduction

Local acute inflammation in living organisms is a mechanism of defense in response to a tissue lesion or against an invasion of microbial pathogens. If it gets out of control, it evolves into chronic and may lead to a wide range of diseases that can be attributed to a failure of resolution. So, inflammatory processes are a first-order health problem.[1]

The inflammatory response begins with the action of the phospholipase enzymes acting over the phospholipids in the cell membranes to free several polyunsaturated fatty acids such as the ω-6 arachidonic acid (AA, 5*Z*,8*Z*,11*Z*,14*Z*-eicosatetraenoic acid), and the fatty acids ω-3 eicosapentaenoic (EPA) and docosahexaenoic (DHA). These fatty acids start a series of synthetic routes where several enzymes are at play. The specialized pro-resolving lipid mediators (SPMs),[2] which are cell signaling molecules formed in cells by the metabolism of polyunsaturated fatty acids, are crucial for causing the resolution of inflammation, so alleviating chronic inflammatory diseases.[3]

5*S*,6*R*,15*S*-trihydroxy-7*E*,9*E*,11*Z*,13*E*-eicosatetraenoic acid and 5*S*,14*R*,15*S*-trihydroxy-6*E*,8*Z*,10*E*,12*E*-eicosatetraenoic acid were the first SPMs discovered. These products (Figure 1) are now termed lipoxinA_4 (LXA_4) and lipoxinB_4 (LXB_4),[4,5] respectively, and derive from AA. The biosynthesis of these lipoxins (lipoxygenase interaction products) requires catalysis by lipoxygenases. Lipoxygenases (LOXs) are a family of non-heme, non-sulfur iron dioxygenases that catalyze the highly regio- and stereospecific hydroperoxidation of polyunsaturated fatty acids containing 1,4-Z,Z-pentadiene units.[6–10] Cells can employ a number of biosynthetic pathways for producing lipoxins, depending on the available LOX isoenzymes and the available substrates. However, the molecular details of the mechanisms of these pathways are not well understood yet.

One of the most important biosynthetic pathways involves 5(*S*),15(*S*)-dihydroperoxyeicosatetraenoic acid (5(*S*),15(*S*)-diHpETE), an intermediate identified in a variety of biological samples (Figure 1).[11] 5(*S*),15(*S*)-diHpETE is produced from AA by two successive hydroperoxidations catalyzed by the enzymes 15-LOX-1 and 5-LOX each. Holman and coworkers[11] have shown that human reticulocyte 15-LOX-1 is 20-fold more efficient than human platelet 12-LOX in catalyzing the production of LXB_4 from 5*S*,15*S*-diHpETE. This is quite surprising because the reaction is initiated by the abstraction of a C_{10} hydrogen atom from 5(*S*),15(*S)*-diHpETE by the Fe^{III} - OH^- cofactor of the enzyme, and C_{10} is the preferential hydrogen abstraction position for 12-LOX, but not for 15-LOX-1. Also, three intriguing points related to 15-LOX-1 catalysis remain unsolved:

a) After the C_{10} hydrogen abstraction, two possible competitive mechanisms can be envisaged to produce lipoxins. The first one, dehydration or epoxidation, consists of either 5,6-epoxide or 14,15-epoxide formation followed by the opening of the corresponding epoxide catalyzed by a hydrolase, leading to LXA_4 or LXB_4, respectively (see Figure 1). The second one, oxygenation, involves the addition of an oxygen molecule at C_6 or C_{14}, formation of the corresponding hydroperoxide, and reduction to LXA_4 or LXB_4, catalyzed by a reductase. The experimental results by Holman and coworkers[11] have been explained by suggesting no preference for any of these two mechanisms. However, although the presence of hydroperoxides was clearly demonstrated, no epoxide was directly detected. Besides, Kühn et al.[12] had previously shown that LXB_4 could be formed by oxygenation of 5(*S*),15(*S*)-diHpETE methyl ester catalyzed by rabbit reticulocyte 15-LOX-1, without the formation of an epoxide.

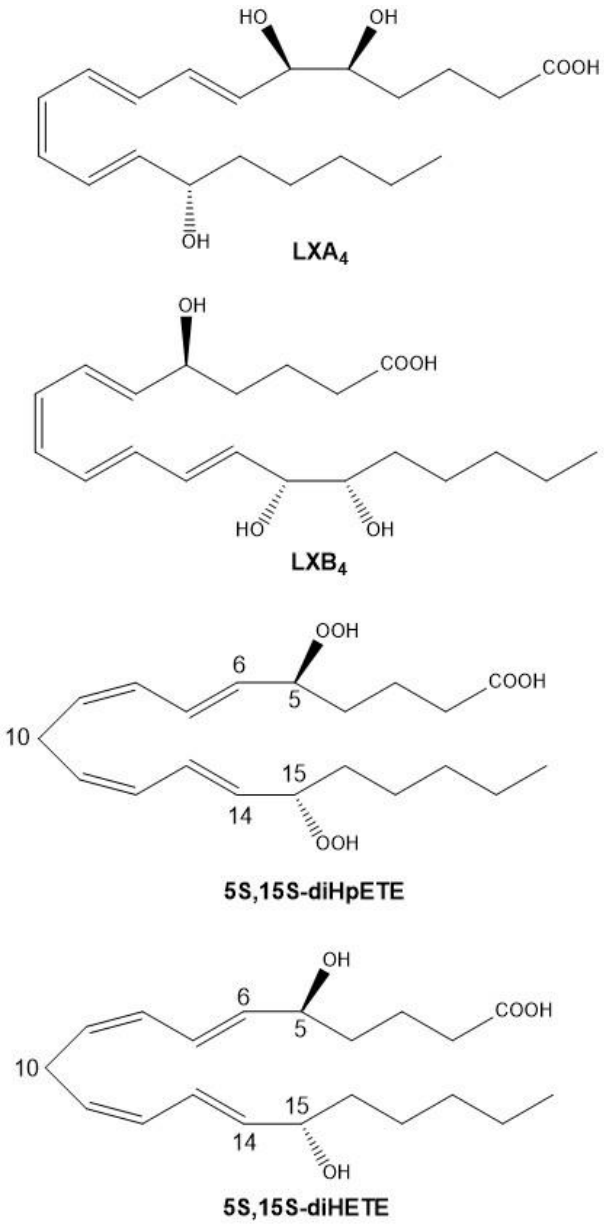

Figure 1. Structures corresponding to (from top to bottom) LXA_4, LXB_4, 5(*S*,15(*S*)-diHpETE and 5(*S*),15(*S*)-diHETE.

b) 15-LOX-1 only produces LXB_4 from 5(*S*),15(*S*)-diHpETE, but not LXA_4.[11]

c) 15-LOX-1 is unable to catalyze any oxygenation reaction with 5(*S*),15(*S*)-dihydroxyeicosatetraenoic acid (5(*S*),15(*S*)-diHETE) (Figure 1), the reduced form of 5(*S*),15(*S*)-diHpETE, which cannot form epoxides.[11]

In this paper, we intend to progress in understanding at a molecular level the lipoxin formation mechanism by means of the 5(*S*),15(*S*)-diHpETE biosynthetic pathway. To this aim, we have combined molecular dynamics (MD) simulations and quantum mechanics/molecular mechanics (QM/MM) calculations to explore the different reactions that reticulocyte 15-LOX-1 is able to catalyze when either 5(*S*),15(*S*)-diHpETE or 5*S*,15*S*-diHETE act as the substrate. The results can be useful to better comprehend how the pro-resolving lipid mediators are biosynthesized.

2. COMPUTATIONAL METHODS

2.1. Protein Setup

The crystallographic x-ray structure of human 15-LOX-1 has not been reported yet. However, it is known that rabbit 15-LOX-1 has approximately 80% sequence identity[13] with the human one. So, the x-ray structure of rabbit 15-LOX-1 dimer (PDB code: 2P0M)[14] was processed, removing monomer A and the ligand bound at the active site of monomer B. The protein was protonated with the H++ web-server.[15,16] A pH = 6.5 for the titrable residues was employed. The protonation state for the iron coordination sphere was corrected by hand for monomer B in order to ensure a correct description of it.

2.2. Molecular docking simulations

The program GOLD5.2.2[17] was employed to carry out docking calculations for 5(*S*),15(*S*)-diHETE and 5(*S*),15(*S*)-diHpETE within the pocket of the monomer B mentioned above. During the conformational search, the protein was treated as a rigid receptor while a complete flexibility was given to the ligand. The GOLD's option to take

into account the interactions of organic ligands with metal ions in metalloenzymes was activated, but restricting the docking exploration to hexacoordinated geometries of iron. The conformational space of both substrates was explored using the genetic algorithm. The binding site was defined as a 20 Å radius sphere centered on the iron atom. Binding free energies were estimated by the ChemScore fitness function.

2.3. Molecular Dynamics simulations

The best two poses for each ligand were selected to run an MD simulation with each one. The recommended procedure by the AMBER program package[18] was used to assemble different systems. The resulting systems contain nearly 86500 atoms of which about 10600 belong to the protein. The rest of atoms correspond to water molecules and salt ions. Additional details of the MD simulations are given in the Supporting Information.

2.4. QM/MM Calculations

The modular program package ChemShell[19,20] was employed to carry out the QM/MM calculations. TURBOMOLE[21] was used for the DFT calculations, while AMBER force fields were employed for the MM calculations by using the DL_POLY[22] module in ChemShell. An electronic embedding scheme[23] was employed to treat the interaction between the QM and MM subsystems. Moreover, a link atom scheme was adopted to describe the QM/MM boundary by using the charge shift model.[24] Finally, cutoffs were not introduced to treat the nonbonding MM and QM/MM interactions.[25]

The active region was defined by all residues and water molecules inside a 15 Å radius sphere centered on C_{10} of the ligand molecule. This region was allowed to move freely (≈ 2100 atoms) while the atoms left were kept frozen. Roughly 12000 atoms were taken into account in the QM/MM calculations. As for the hydrogen abstractions and the

epoxide formations, the QM region (Figure 2) was defined by all atoms of the lipid substrate which are found between C_4 and C_{16}, 11 atoms for each His residue in the iron coordination sphere (His361, His366, His541 and His545), 3 atoms of the Ile terminal residue (Ile 663) in the iron coordination sphere and the Fe^{III} - OH^- cofactor, whereas for oxygenations and the hydrogen retrodonation, this region was enlarged by an oxygen molecule.

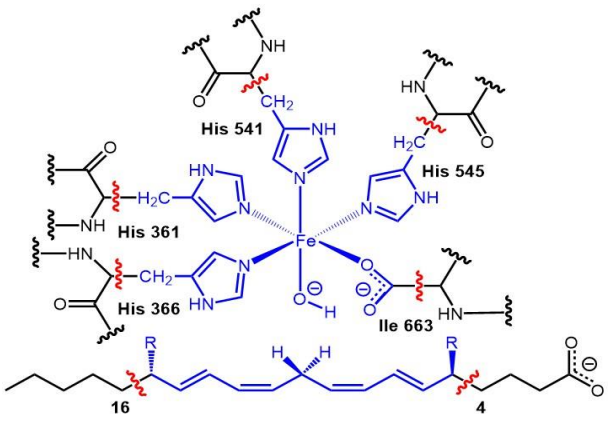

Figure 2: QM/MM partition for the hydrogen abstractions and the epoxide formations. QM atoms are depicted in blue. The boundary between QM and MM regions is indicated by red wavy lines. R is OOH for 5(*S*),15(*S*)-diHpETE or OH for 5(*S*),15(*S*)-diHETE.

Seven link atoms were employed, five between the bonds Cα-QM atoms of the five residues in the iron coordination sphere and two bonded to the aliphatic carbon atoms of the lipid substrate (placed between C_4-C_5 and C_{15}-C_{16}). A complete view of the 5(*S*),15(*S*)-diHpETE: rabbit 15-LOX-1 Michaelis complex is pictured in Figure 3. Additional details of the QM/MM calculations are given in the Supporting Information.

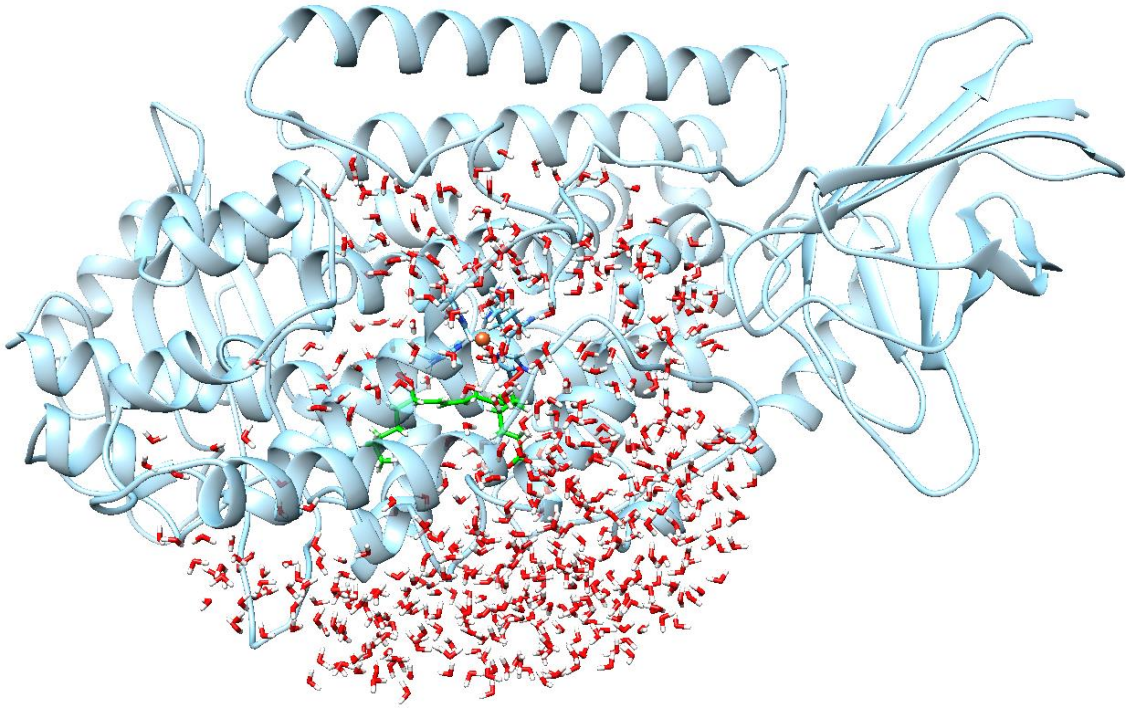

Figure 3: A complete view of the 5(*S*),15(*S*)-diHpETE:rabbit 15-LOX-1 Michaelis complex. Carbon atoms of the substrate are pictured in green, and oxygen atoms are in red. The Fe is in gold and the nitrogen atoms of the His residues of its coordination sphere are depicted in dark blue. The water molecules inside a 17 Å radius volume centered on the substrate molecule are shown. All hydrogen atoms represented are in white.

2.5. Tunnel Search

The oxygen access channels have been searched using the Caver3.0 program[26] and analyzing the first 2000 frames of the first MD simulation for each ligand. In all systems, the substrate location was used as the initial starting point to compute the tunnels. We selected the default settings for the calculation of protein channels, except for the minimum probe radius, which has been set to a value of 2 Å. All visualizations and pictures were performed with VMD[27] and UCSF CHIMERA[28] programs.

3. RESULTS AND DISCUSSION

3.1. Molecular docking simulations of 5(*S*),15(*S*)-diHpETE and 5(*S*),15(*S*)-diHETE

All docking calculations set the substrate tail first. Tail-first orientation means that the incoming AA methyl group points to the enzyme cavity end. The docking of 5(*S*),15(*S*)-diHpETE has yielded 4 clusters, 2 of which are the most populated. In these two clusters the carboxylate group is close to the Phe175 and Leu408's backbones (NH group). The hydroperoxide group at C_5 of 5(*S*),15(*S*)-diHpETE forms a hydrogen bond with the terminal Ile663 (in the Fe coordination sphere), which in turn is forming a hydrogen bond with the OH group of the Fe^{III} - OH^- cofactor. Furthermore, the hydroperoxide group at C_{15} of 5(*S*),15(*S*)-diHpETE forms hydrogen bonds with Gln548 and Glu357 and is near His361 (see Figures 4a and S1).

The docking of 5(*S*),15(*S*)-diHETE has yielded 8 clusters, 2 of which are also the most populated. In these two clusters the carboxylate group is also close to the Phe175 and Leu408's backbones (NH group). The hydroxyl group at C_5 is forming a hydrogen bond with Ile663 or with Ile400, depending on the main cluster chosen. On the other hand, the hydroxyl group at C_{15} forms hydrogen bonds with Gln548 and Glu357, and is near His361 (see Figures 4b and S2).

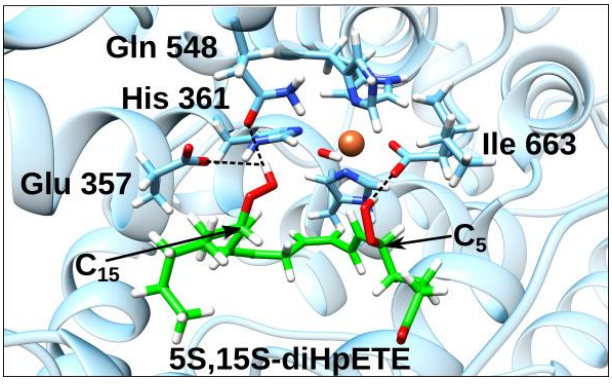

a)

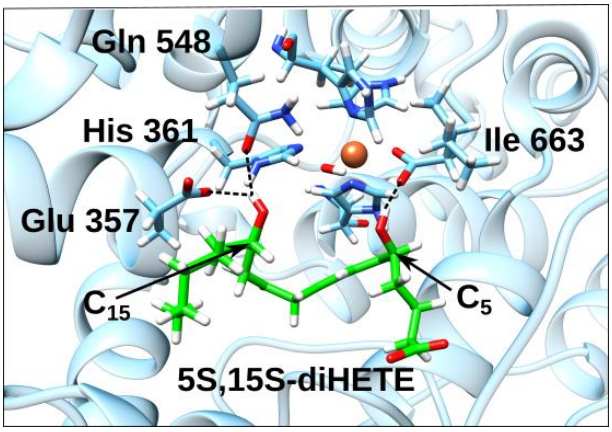

b)

Figure 4: Representative structure of the most populated cluster corresponding to the docking of 5(*S*),15(*S*)-diHpETE (a) and the docking of 5(*S*),15(*S*)-diHETE (b).

3.2. Molecular dynamics simulations of 5(*S*),15(*S*)-diHpETE and 5(*S*),15(*S*)-diHETE

Two 100 ns molecular dynamics simulations of the 15-LOX-1:5(*S*),15(*S*)-diHpETE Michaelis complex plus two more of the 15-LOX-1:5(*S*),15(*S*)-diHETE Michaelis complex have been carried out. Each one starts, respectively, from structures that are representative of the 4 most populated clusters mentioned above. Instead of detailing the results for every MD, the general features will be explained (see Figure 5).

The analyses of the results indicate that there are not significant differences between the binding modes for both substrates if just the identity of their closest residues is considered. The carboxylate group forms hydrogen bonds, which are not preserved in all MDs, with different residues that are found on the pocket entrance. Phe175, Arg403 and Leu408 seem to have a main role in the carboxylate binding.

Both the hydroperoxide group and the hydroxyl group at C_{15} form a hydrogen bond with Glu357, which is also forming a hydrogen bond with His361 (in the Fe coordination sphere). Moreover, Gln548 also interacts with the substituent at C_{15}. Besides, Leu597 is close to the substituent at C_{15} in both substrates.

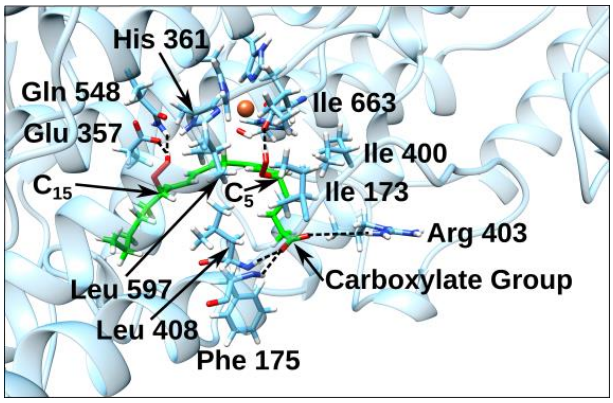

a)

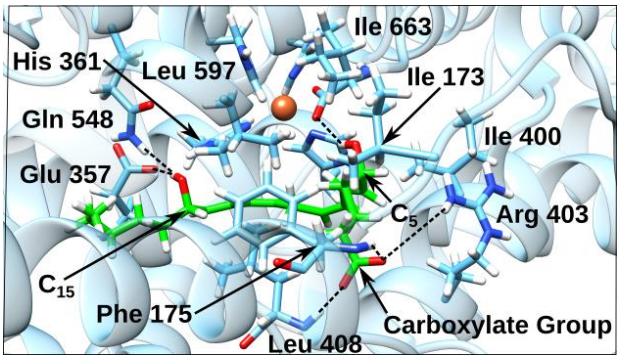

b)

Figure 5: Representative structure of the MD simulation starting from the most populated cluster corresponding to the docking of 5(*S*),15(*S*)-diHpETE (a) and the docking of 5(*S*),15(*S*)-diHETE (b).

The substituent at C_5 forms a hydrogen bond with the terminal Ile663, which is forming a hydrogen bond with the OH group in the Fe coordination sphere. Additionally, Leu597, Ile173 and Ile400 are placed close to this substituent.

However, the different type of substituents when comparing 5(*S*),15(*S*)-diHpETE and 5(*S*),15(*S*)-diHETE provokes some subtle differences in the relative positions of the substrates and the residues. See, for instance, that Figures 5a and 5b are far to overlap.

Finally, due to the different nature of the substituents (-OH versus -OOH) at C_5 and C_{15} positions, the diHETE's carbon backbone is closer to the Fe coordination sphere than the diHpETE's one. This fact can make substrate reorganization more difficult in the case of diHETE.

On the other hand, the first step of the 15-LOX-1 catalyzed reaction for any of the two substrates must be the abstraction of a C_{10} hydrogen atom. So, it is worth analyzing the evolution of the distances between the relevant atoms along the molecular dynamics simulations. As for the distance between C_{10} and the oxygen atom of the Fe^{III} - OH^- cofactor of 15-LOX-1 (C_{10} - O, see Figure 6), the pictures of the four MD simulations roughly match. C_{10} almost always holds quite close to the proton acceptor oxygen atom, the corresponding distance fluctuating around 3.5 Å. The average distances C_{10} - O (see Table 1) reflect this fact. On the other hand, there is almost always a hydrogen atom bonded to C_{10} as near as 2.5 Å to 3 Å from the proton acceptor oxygen atom, or even closer. This atom is almost exclusively $H_{10pro\mathit{S}}$ for the two MD simulations corresponding to the 15-LOX-1:5(*S*),15(**S**)-diHpETE Michaelis complex (see Figure 7), as the corresponding average distances (see Table 1) indicate. However, the closest hydrogen atom is mostly $H_{10pro\mathit{R}}$ for the first MD simulation corresponding to the 15-LOX-1:5(*S*),15(*S*)-diHETE Michaelis complex, but almost exclusively $H_{10pro\mathit{S}}$ for the second MD simulation (see Figure 8). These results show that C_{10} rotates during this first MD

simulation, so exchanging the positions of its two attached hydrogen atoms with respect to the proton acceptor oxygen atom. This rotation causes that the average distance corresponding to the closest hydrogen atom is somewhat bigger (3.19 Å) than in the other cases (see Table 1). Moreover, the position of C_{10} has clearly rotated when comparing the first with the second MD simulation. Because C_{10} does not turn during this second MD simulation, the average distance $H_{10pro\mathit{S}}$ -O is now shorter (2.77 Å) and comparable with the two of cases 5(*S*),15(*S*)-diHpETE (see Table 1). The percentage of precatalytic structures (structures where at least one hydrogen atom at C_{10} is closer than 3.0 Å from the oxygen atom of the Fe^{III} - OH^- cofactor) throughout each 100 ns molecular dynamics simulation is also shown in Table 1. Thus, many of the structures generated along the four MDs seem suitable to undergo the abstraction of one C_{10} hydrogen atom as far as a criterion of distances is concerned. Likewise, the average d($H_{10pro\mathit{S}}$ -O) is clearly smaller than the average d($H_{10pro\mathit{R}}$ -O). As mentioned in the Introduction, 15-LOX-1 cannot catalyze the oxygenation reaction of 5(*S*),15(*S*)-diHETE. However, according to our results so far, 5(*S*),15(*S*)-diHETE and 5(*S*),15(*S*)-diHpETE show a similar trend for the hydrogen abstraction from C_{10}. So, QM/MM calculations are needed to explain the different reactivity of 5(*S*),15(*S*)-diHpETE.

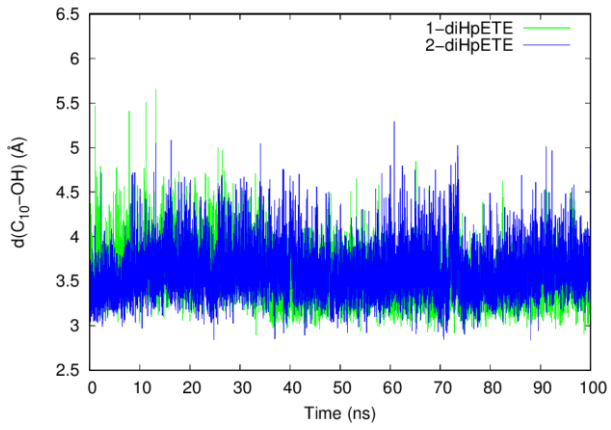

a)

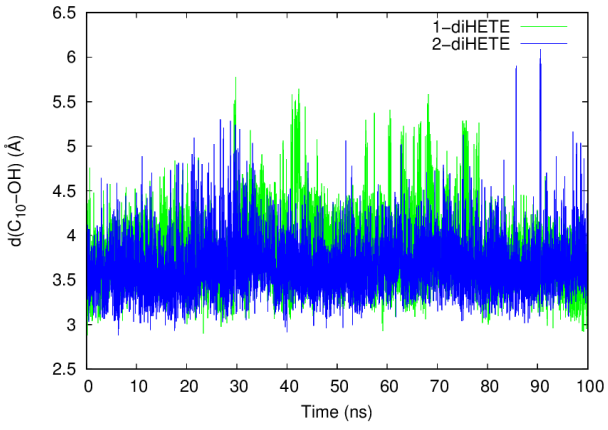

b)

Figure 6. Distances C_{10} - O (in Å) along the molecular dynamics simulation for a) the 15-LOX-1:5(S),15(S)-diHpETE Michaelis complex and b) the 15-LOX-1:5(*S*),15(*S*)-diHETE Michaelis complex. The first and second MD simulations for each case are pictured in green and blue, respectively. O stands for the oxygen atom of the Fe^{III} - OH^- cofactor of 15-LOX-1.

a)

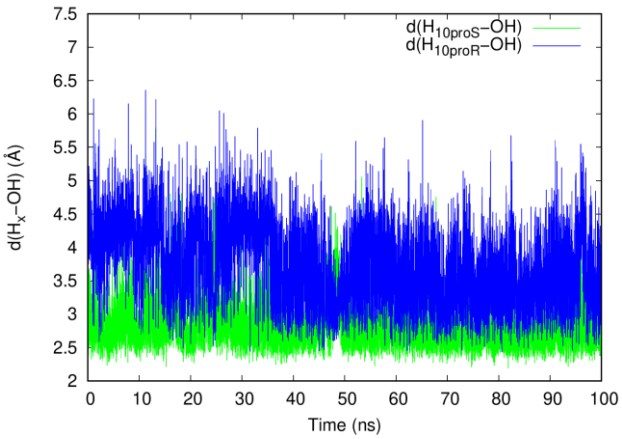

b)

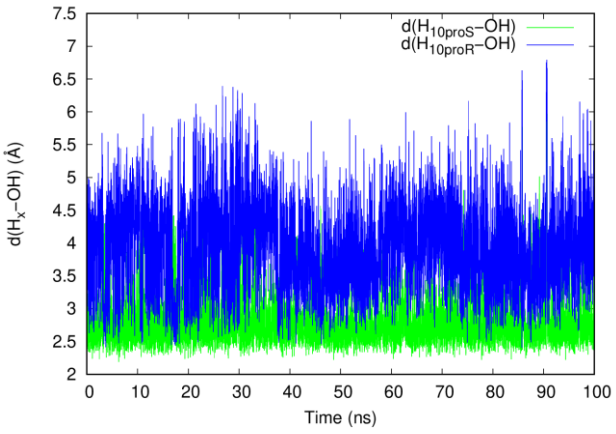

Figure 7. Distances H_{10proS} - O (green line) and H_{10proR} - O (blue line) (in Å) along the first (a, 1-diHpETE) and second (b, 2-diHpETE) molecular dynamics simulation for the 15-LOX-1:5(*S*),15(*S*)-diHpETE Michaelis complex**.** O stands for the oxygen atom of the Fe^{III} - OH^- cofactor of 15-LOX-1. H_{10proS} and H_{10proR} are the hydrogen atoms attached to C_{10}.

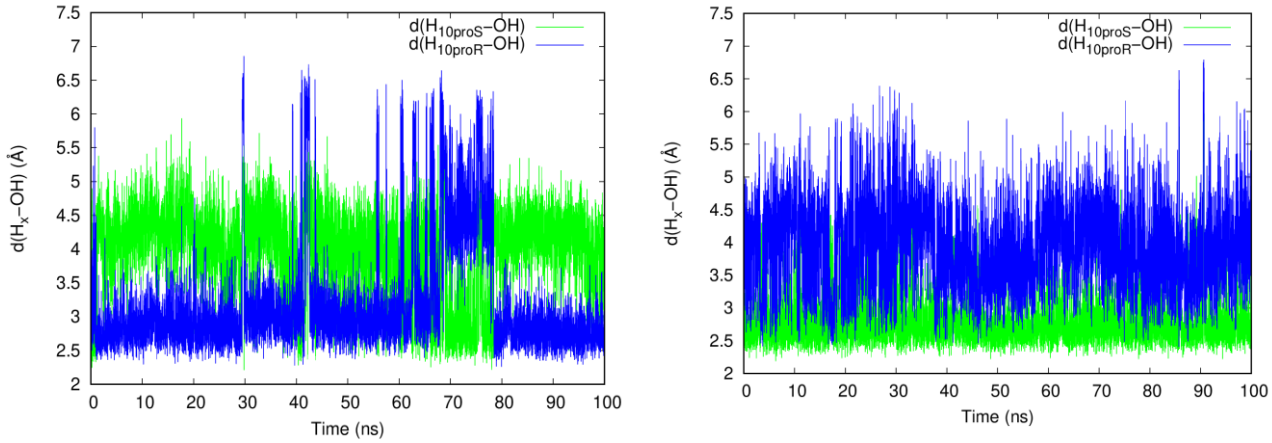

a) b)

Figure 8. Distances $H_{10pro\mathit{S}}$ - O (green line) and $H_{10pro\mathit{R}}$ - O (blue line) (in Å) along the first (a, 1-diHETE) and second (b, 2-diHETE) molecular dynamics simulation for the 15-LOX-1:5(*S*),15(*S*)-diHETE Michaelis complex**.** O stands for the oxygen atom of the Fe^{III} - OH^- cofactor of 15-LOX-1. $H_{10pro\mathit{S}}$ and $H_{10pro\mathit{R}}$ are the hydrogen atoms attached to C_{10}.

Table 1. Average distances (in Å) between the atoms that directly intervene in the abstraction of a C_{10} hydrogen atom, and percentage of the precatalytic structures, for the four molecular dynamics simulations.[a]

MD simulation	d(C_{10}-O)	d($H_{10pro\mathit{S}}$ -O)	d($H_{10pro\mathit{R}}$ -O)	Precatalytic structures percentage
1-diHpETE	3.54	2.79	3.73	83.7
2-diHpETE	3.60	2.86	4.04	79.4
1-diHETE	3.81	3.96	3.19	69.7
2-diHETE	3.64	2.77	3.92	86.4

[a]1-diHpETE and 2-diHpETE correspond to the two MD simulations with the substrate 5(*S*),15(*S*)-diHpETE; 1-diHETE and 2-diHETE correspond to the two MD simulations with the substrate 5(*S*),15(*S*)-diHETE; $H_{10pro\mathit{S}}$ and $H_{10pro\mathit{R}}$ are the hydrogen atoms attached to C_{10}; O stands for the oxygen atom of the Fe^{III} - OH^- cofactor of 15-LOX-1; and the last column indicates the percentage of precatalytic structures (structures where at least one hydrogen atom at C_{10} is closer than 3.0 Å from the oxygen atom of the Fe^{III} - OH^- cofactor) that appear throughout each 100 ns molecular dynamics simulation.

3.3. QM/MM calculations

For the sake of clarity, we have shown the set of reactions we have studied in this paper with 5(*S*),15(*S*)-diHpETE (Figure 9) and 5(*S*),15(*S*)-diHETE (Figure 10) as substrates.

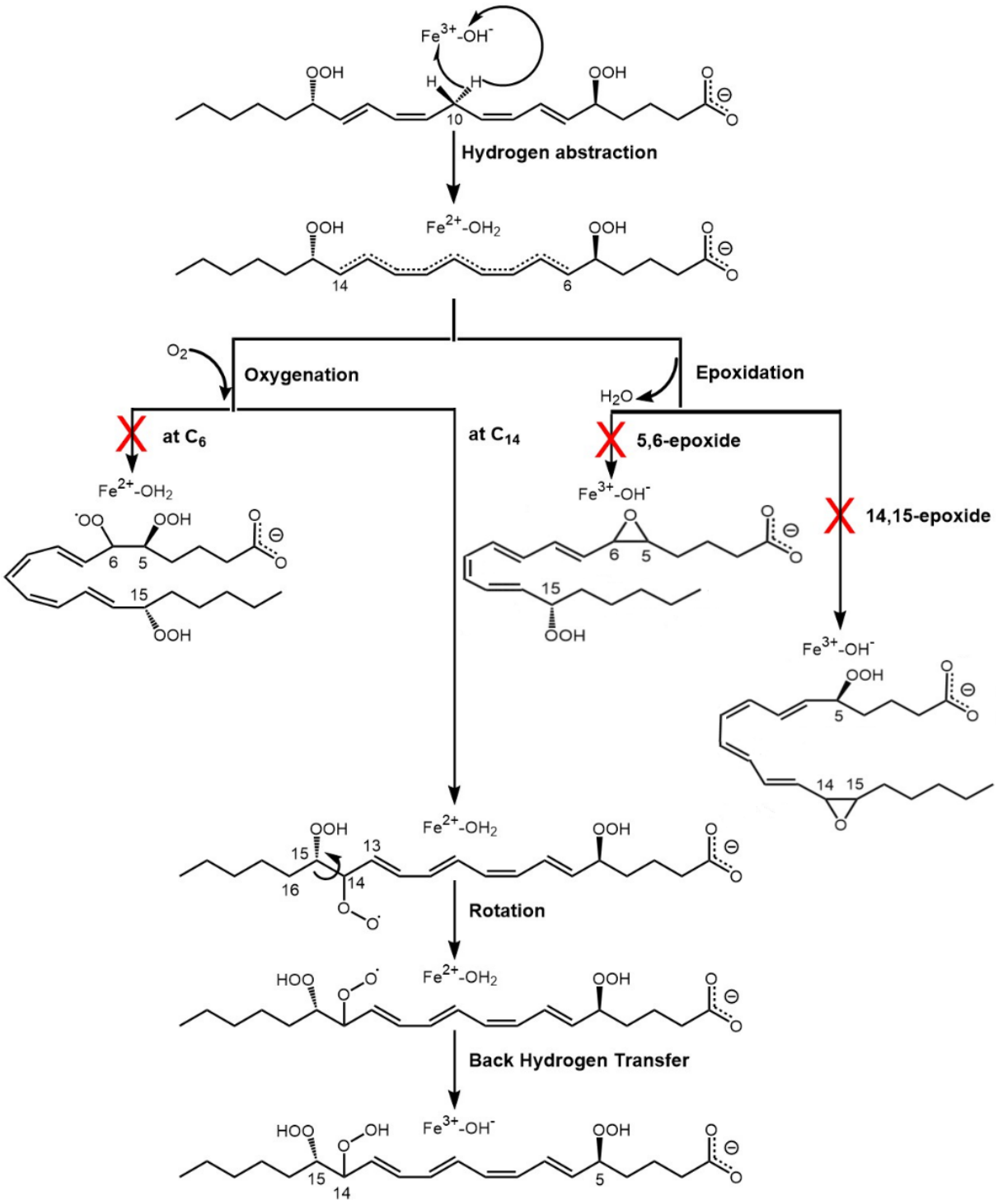

Figure 9: Set of reactions we have studied in this paper with 5(*S*),15(*S*)-diHpETE as substrate. The red marks highlight those reaction pathways that our calculations predict as unfeasible.

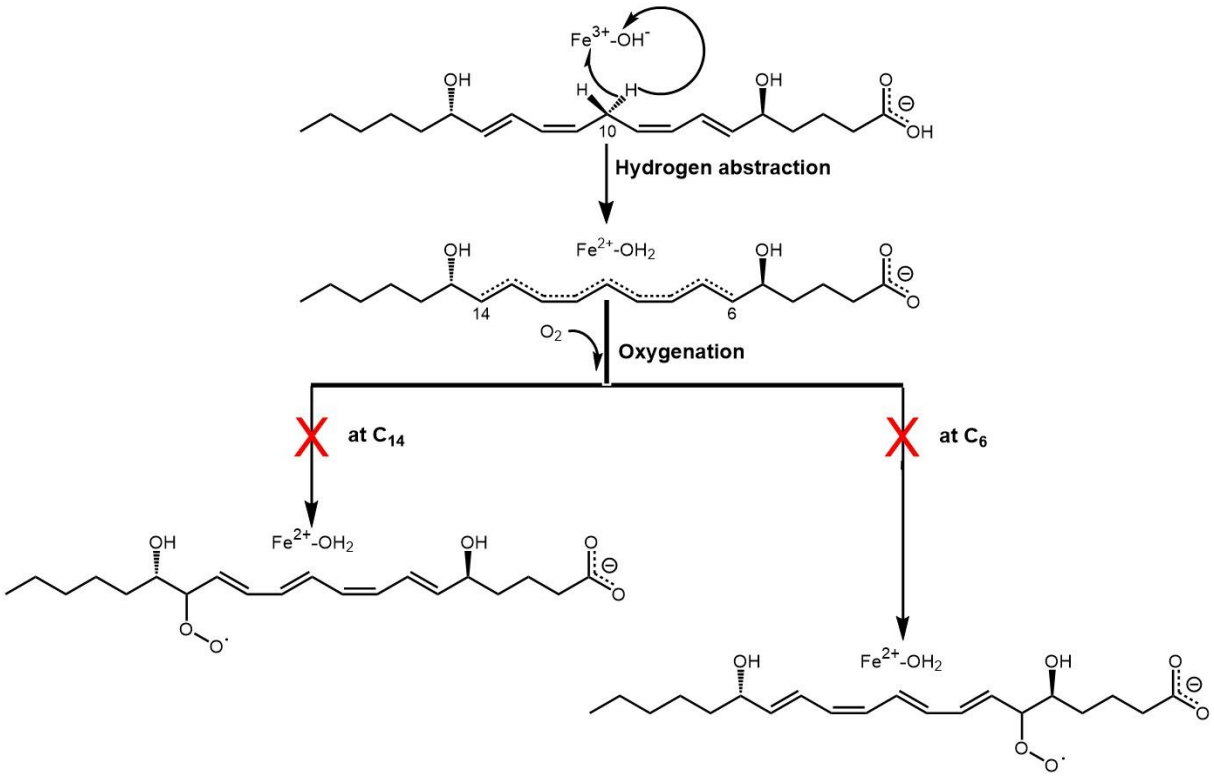

Figure 10: Set of reactions we have studied in this paper with 5(*S*),15(*S*)-diHETE as substrate. The red marks highlight those reaction pathways that our calculations predict as unfeasible.

3.3.1. Abstraction of a C_{10} hydrogen atom from 5(*S*),15(*S*)-diHpETE and 5(*S*),15(*S*)-diHETE

We have selected one precatalytic structure for each one of the MDs we have carried out. In each case, the hydrogen atom at C_{10} closest to the proton acceptor oxygen atom has been chosen to be abstracted ($H_{10pro\mathit{S}}$). Starting from the optimized geometry corresponding to each structure the corresponding potential energy profile has been calculated as a function of the reaction coordinate (see Figure 11). This reaction

coordinate has been defined as the difference between the breaking bond length (C_{10} - H_x) and the forming bond length (H_x - O). The transition state structures were located from the maximum energy point of each profile. The resulting potential energy barriers turn out to be 9.6 kcal/mol and 9.3 kcal/mol for the substrate 5(*S*),15(*S*)-diHpETE, and 10.5 kcal/mol and 12.6 kcal/mol for the substrate 5(*S*),15(*S*)-diHETE. These values indicate that the hydrogen atom at C_{10} is slightly easier to abstract in the case of 5(S),15(S)-diHpETE, but the difference is too small to explain why 5(*S*),15(*S*)-diHETE is not oxidized.

It is interesting to compare these reactions with the case of AA as substrate of 15-LOX-1. When a C_{13} hydrogen atom of AA is abstracted, a planar system of five electrons delocalized over the five carbon atoms (C_{11} - C_{15}) of a π-pentadienyl radical is formed. An exponential average potential energy barrier of 19.6 kcal/mol was calculated[29] for this reaction. In contrast, the product of the hydrogen abstraction in the case of 5(*S*),15(*S*)-diHpETE and 5(*S*),15(*S*)-diHETE contains a planar system of nine electrons delocalized over the nine carbon atoms (C_6 - C_{14}) of a π nonatetraenyl radical. This more extended conjugation of the π radical in the product contributes to remarkably lower the abstraction barrier. Moreover, the reaction energies of this step are quite exoergic (around -25 kcal/mol). The geometries of the stationary points corresponding to the potential energy profiles pictured in Figure 11 are shown in Figures S3 to S14.

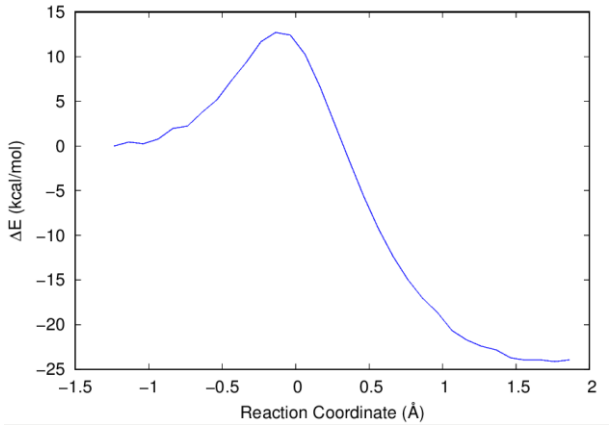

a)

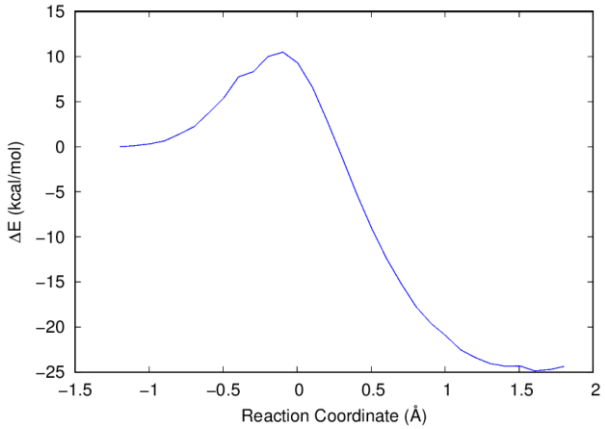

b)

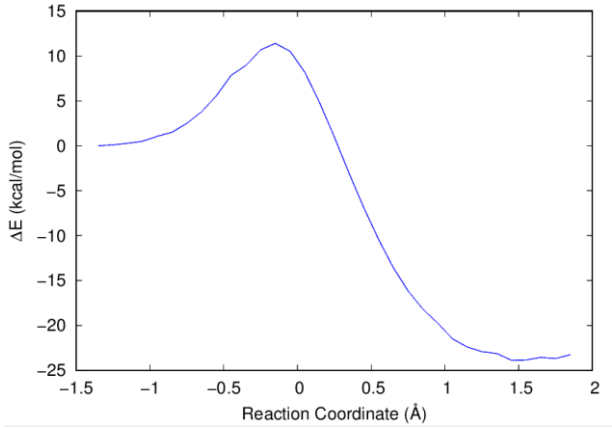

c)

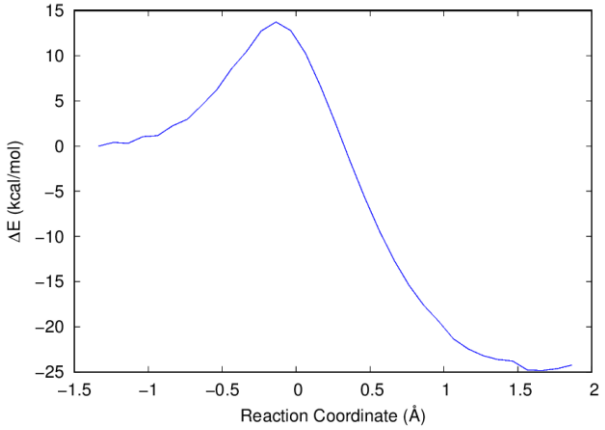

d)

Figure 11. Potential energy profiles for the abstraction of a hydrogen atom from C_{10}. a) and b) correspond to the two structures selected for 5(*S*),15(S)-diHpETE (1-diHpETE and 2-diHpETE, respectively). c) and d) correspond to the two structures selected for 5(*S*),15(*S*)-diHETE (1-diHETE and 2-diHETE, respectively).

3.3.2. Dehydration mechanism

As mentioned in the introduction, after the C_{10} hydrogen abstraction, two possible competitive mechanisms have been proposed to produce lipoxins. In this section we will study the feasibility of the dehydration mechanism. It begins with either 5,6-epoxide or 14,15-epoxide formation, leading finally to LXA_4 or LXB_4, respectively. Because

5(*S*),15(*S*)-diHETE cannot form epoxides we will now focus only on 5(*S*),15(*S*)-diHpETE.

We have first tried to form the 14,15-epoxide derived from 5(*S*),15(*S*)-diHpETE (see Figure 1). Brash and coworkers[30] and Holman and coworkers[31] have suggested a mechanism for formation of epoxides in 5-HpETE catalyzed by 5-LOX. After a C_{10} hydrogen abstraction from 5-HpETE, a homolytic cleavage of the hydroperoxide at C_5 occurs, the Fe^{II} - OH_2 cofactor transfers a hydrogen atom to the nascent hydroxyl radical to form a water molecule and the 5,6-epoxide is cycled by radical recombination. We have explored if this mechanism is also valid in the current case with 15-LOX-1. Since both products of the C_{10} hydrogen abstraction from 5(*S*),15(*S*)-diHpETE obtained before (see section 3.3.1. and Figures S5 and S8) are quite similar, the optimized geometry corresponding to one of them has been taken as the starting point to calculate a potential energy profile for the epoxidation. A number of reaction coordinates were tested. In this process 2 bonds are formed and 2 bonds are broken. We have used different linear combinations of 4, 3 or 2 of these bonds to define the reaction coordinate. All of them involved huge energy barriers. The least energy costly reaction coordinate (see the corresponding potential energy profile in Figure 12) turned out to be the difference between the length of the breaking bond O - O of the hydroperoxide at C_{15} and the length of the nascent bond O (hydroperoxide) - C_{14}. Along this reaction coordinate, the O - O breakage, the epoxide formation and the hydrogen transfer to form water and the cofactor Fe^{III} - OH^- should take place synchronically. The epoxide appears placed in a suprafacial situation with respect to the cofactor. Even in this case, the potential energy barrier is as high as 35.1 kcal/mol. The process is endoergic, with a reaction energy of 10.6 kcal/mol.

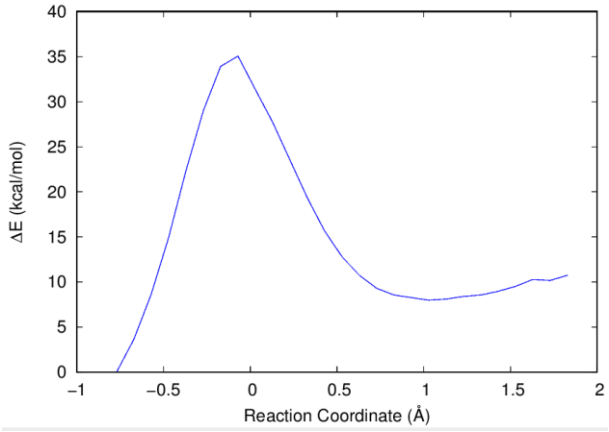

Figure 12. Potential energy profile corresponding to the formation of the 14,15-epoxide derived from 5(*S*),15(*S*)-diHpETE.

To ensure that there not exists a more favourable pathway, a bidimensional potential energy surface as a function of the O - O bond length and the O (hydroperoxide) - C_{14} length was calculated (see Figure 13). In this 2D-surface the reactant is placed at the upper left corner and the epoxide at the lower right corner. The diagonal of the 2D-surface corresponds to the potential energy profile shown in Figure 6. As a matter of fact, no reaction path can be traced on the 2D-surface that involves a potential energy barrier lesser than roughly 35 kcal/mol. Hence, this result does not predict that 15-LOX-1 catalyzes the formation of the 14,15-epoxide from 5(*S*),15(*S*)-diHpETE. Structurally, looking at the product of the C_{10} hydrogen abstraction (see Figure S5), this high barrier is due to the fact that the hydrogen atom to be transferred from the cofactor is too far away (5.8 Å) from the hydrogen acceptor oxygen atom of the hydroperoxide at C_{15}. That is, the cofactor is too far from the hydroperoxide, and the corresponding hydrogen transfer from the cofactor to the nascent hydroxyl radical to form a water molecule is not predicted to be possible. If the water formation were possible, the potential energy barrier would decrease since the water formation stabilizes the process. As a matter of fact, the hydrogen atoms of the Fe^{II} - OH_2 cofactor are oriented towards the hydroperoxide group at C_5 (see

Figure S5), with its oxygen atom placed above the C_9-C_{10} bond (the distance from the hydrogen atom to be transferred to the hydrogen acceptor oxygen atom of the hydroperoxide at C_5 is 3.99 Å) .

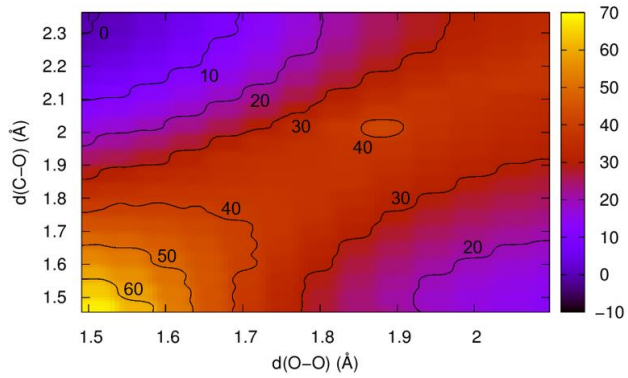

Figure 13. Bidimensional potential energy surface corresponding to the formation of the 14,15-epoxide derived from 5(*S*),15(*S*)-diHpETE.

As for the formation of the 5,6-epoxide, by analogy with the 14,15-epoxide, the difference between the length of the breaking bond O - O of the hydroperoxide at C_5 and the length of the nascent bond O (hydroperoxide) - C_6 has been chosen as reaction coordinate. Along this reaction coordinate the substrate suffers an important reorganisation, especially the dihedral angle defined by the hydrogen atom at C_6, C_6, C_5 and the oxygen atom of the hydroperoxide group at C_5. The O-O bond breaks, but the shortest value that the distance O - C_6 reaches is 2 Å, clearly too large in comparison with the normal C-O bond length in an epoxide (around 1.4 Å). If from this region the distance between C_6 and the O at C_5 is now chosen as a new reaction coordinate and the formation of the 5,6-epoxide (now placed antarafacially regarding to the Fe atom) is forced, and extremely huge potential energy barrier of 71.6 kcal/mol is obtained. Thus, it is clear that 15-LOX-1 is not able to catalyze the formation of the 5,6-epoxide from 5(*S*),15(*S*)-diHpETE. The 5,6-epoxide formation is infeasible because it is hindered by Ile663 (see Figure S5) which is placed

between the Fe^{II} - OH_2 cofactor and the hydroperoxide at C_5, as it has already been mentioned above in the docking and molecular dynamics sections.

At this point we can wonder why 15-LOX-1 is able to catalyze the formation of the 14,15-epoxide from AA as a substrate following the mechanism suggested by Brash and coworkers[30] and Holman and coworkers[31], but our calculations do not predict this formation when the substrate is 5(*S*),15(*S*)-diHpETE. We have analyzed the evolution of the distances between the carbon atoms C_5 or C_{15} and the oxygen atom of the cofactor Fe^{III} - OH^- along the two 100 ns molecular dynamics simulations 1-diHpETE and 2-diHpETE, in comparison with an analogous simulation for AA. The results for C_{15} are pictured in Figure 14. Likewise, the averages of those distances are shown in Table 2.

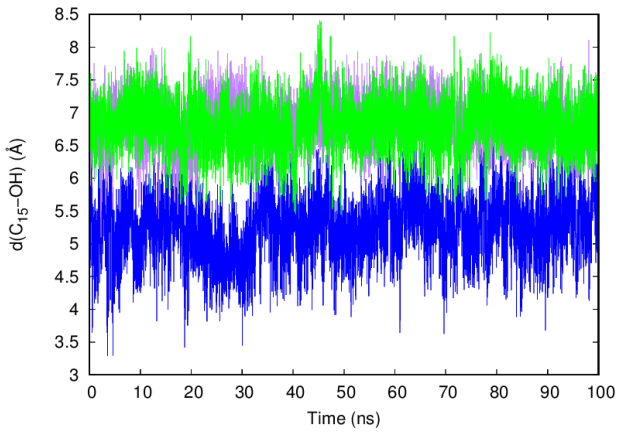

Figure 14: Evolution of the distance between C_{15} and the oxygen atom of the Fe^{III} - OH^- cofactor as a function of time for AA (blue) and 5(*S*),15(*S*)-diHpETE (purple for 1-diHpETE and green for 2-diHpETE).

Table 2: Average distances and standard deviations for C_5 and C_{15} in relation to the oxygen atom of Fe^{III} - OH^- cofactor.

	d(C_5-O) (Å)	d(C_{15}-O) (Å)
AA	-	5.25 ± 0.48
1-diHpETE	5.22 ± 0.35	6.83 ± 0.35
2-diHpETE	5.17 ± 0.26	6.82 ± 0.38

Using a distance criterion we can understand why the formation of the 14,15-epoxide is not predicted to be possible for 5(*S*),15(*S*)-diHpETE in contrast to the AA case as a substrate. In average (Table 2), C_{15} is more than 1.5 Å closer to the oxygen atom of the Fe^{III} - OH^- cofactor in AA than in 5(*S*),15(*S*)-diHpETE. Moreover, visualizing d(C_{15}-OH) as a function of time (Figure 14), it can be seen that in any of the two molecular dynamics simulations 5(*S*),15(*S*)-diHpETE has its 15-hydroperoxyde group closer enough to the Fe^{III} - OH^- cofactor to make the formation of the 14,15-epoxide possible. On the other hand, when AA is the substrate there is a lot of structures in which its C_{15} is quite close to the Fe^{III} - OH^- cofactor, thus allowing the formation of the 14,15-epoxide. On the other hand, as seen in Table 2, according to a distance criterion, the formation of the 5,6-epoxide in the case of 5(*S*),15(*S*)-diHpETE should be as probable as the formation of the 14,15-epoxide in AA. However, as explained above, Ile663 prevents the formation of the 5,6-epoxide in the case of 5(*S*),15(*S*)-diHpETE. As our docking calculations (Figure 4), molecular dynamics simulations (Figure 5) and QM/MM calculations (Figures S3, S4, S5, S6, S7, S8, S15, S16 and S17) indicate, the hydroperoxide group at C_5 of 5(*S*),15(*S*)-diHpETE forms a hydrogen bond with the terminal Ile663 (in the Fe coordination sphere), which in turn is forming a hydrogen bond with the OH group of the cofactor. This is the key point why the Fe atom and its coordination sphere (including the OH group) keep clearly closer to C_5 and its hydroperoxide than to C_{15} and its hydroperoxide.

To sum up, we can conclude that our calculations do not predict the formation of lipoxins from 5(*S*),15(*S*)-diHpETE catalyzed by 15-LOX-1 by means of the dehydration mechanism. This result is compatible with the fact that no epoxide has been directly detected as an intermediate in the catalytic formation of lipoxins from 5(*S*),15(*S*)-diHpETE.

3.3.3. Oxygenation mechanism

3.3.3.1. Search for oxygen access channels

Once considered the dehydration mechanism, we will study the second competitive mechanism, oxygenation. It involves addition of an oxygen molecule at C_6 or C_{14}, followed by reduction to the corresponding hydroperoxide. A necessary previous step to the study of the oxygen molecule addition to the π nonatetraenyl radicals derived from 5(*S*),15(*S*)-diHETE and 5(*S*),15(*S*)-diHpETE by the C_{10} hydrogen abstraction is to determine the channels for oxygen access from the protein surface into the binding pocket.

As for 5(*S*),15(*S*)-diHETE, we have grouped the located channels into 8 clusters, being one of them clearly the most populated. All these channels flow into C_{14}, what it is somewhat surprising because the oxygen addition could in principle occur both at C_6 and at C_{14}. Moreover, the main cluster channel goes through the space in between α2 and α18 (interphase helixes) and remains open along the whole analyzed MD simulation (see Figures 15a and Figure S18).

As for 5(*S*),15(*S*)-diHpETE, the number of located channels is enormous. They have been grouped into 169 clusters, in such a way that the set of them entirely overlaps the protein pocket. In this case, those channels flow into C_{14} and C_6. However, the main cluster channel mostly flows into C_{14} (see Figure 15b and Figure S19). Unfortunately, neither of

the two nonatetraenyl radicals (see Figures S5 and S8) derived from 5(*S*),15(*S*)-diHpETE by the C_{10} hydrogen abstraction in Section 3.3.1. have the main cluster channel open. Thus, another precatalytic structure was extracted from the first molecular dynamics simulation of the 15-LOX-1:5(*S*),15(*S*)-diHpETE Michaelis complex, now with the main cluster oxygen channel open, and the C_{10} hydrogen abstraction was repeated. The potential energy barrier up to the transition state structure turned out to be 9.3 kcal/mol, and again a planar system of nine electrons delocalized over the nine carbon atoms (C_6 - C_{14}) of a π nonatetraenyl radical was obtained. The structures of the corresponding stationary points are depicted in Figures S15 to S17.

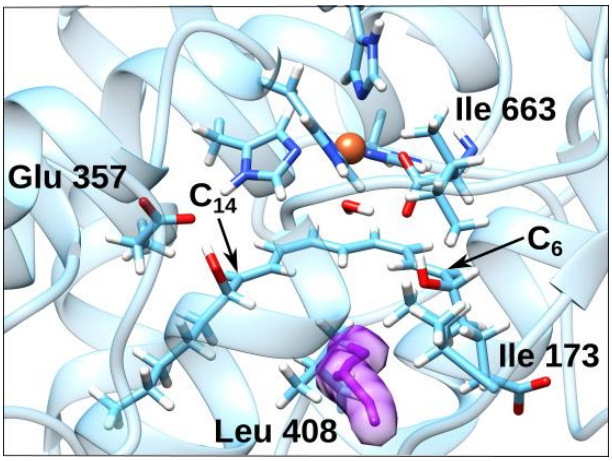

a)

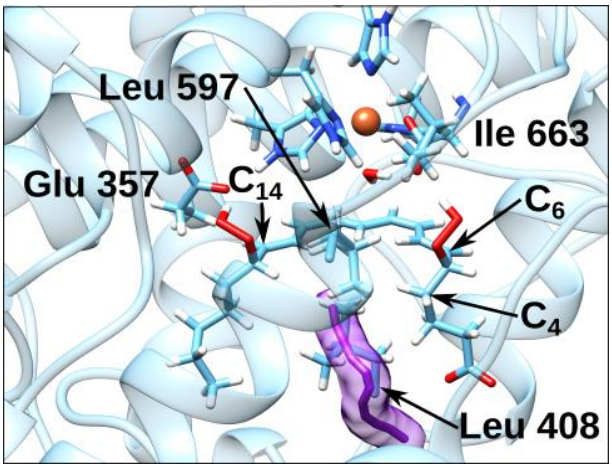

b)

Figure 15. Representative oxygen molecule channel corresponding to the main cluster (in violet) for the case of a) 5(*S*),15(*S*)-diHETE, and b) 5(*S*),15(*S*)-diHpETE. Fe is colored in gold.

3.3.3.2. Oxygen molecule addition

Once the channels through which the oxygen molecule addition can take place have been found for both substrates, one of the products of the hydrogen abstraction step located in section 3.3.1. for 5(*S*),15(*S*)-diHETE (see Figure S11) and the new product located (see Figure S17) in section 3.3.3.1. for 5(*S*),15(*S*)-diHpETE have been used to place an oxygen molecule in the open channel belonging to the most populated cluster for each substrate.

Only the oxygenations to C_{14} have been initially considered since the main cluster channel flows clearly into C_{14}. The oxygen molecule was initially placed at around 6 Å from C_{14}. These hydrogen abstraction products with the oxygen molecule have been fully QM/MM optimized, just keeping frozen the distance between the closest oxygen atom of the incoming oxygen molecule and C_{14} (d(C_{14}-O)). These optimized structures have been employed as the starting points to construct the potential energy profiles for the oxygen attack in which d(C_{14}-O) has been defined as the reaction coordinate.

As for 5*S*,15*S*-diHETE, it can be seen that Leu408, Ile414, Ile593, Ile173, Asp174, Phe175 and Gln596 limit the diameter of the channel through which the oxygen molecule approaches suprafacially (see Figure 15a and Figure S18). Additionally, the diameter of this channel is quite large so that it could contain some water molecules as well as the oxygen molecule. In fact, in this case there is a water molecule inside which is forming a hydrogen bond with the oxygen molecule. In order to correctly describe this interaction, this water molecule had to be added to the QM region. During the oxygen addition, there is an important reorganization between the oxygen molecule and this water molecule, in such a way that the hydrogen bond between them is preserved along the whole oxygen addition, what stabilizes it. Moreover, the oxygen molecule's approach to C_{14} is suprafacial what causes a great distortion in C_{14} giving rise to the formation of a cis bond between C_{12} and C_{13}. As a consequence, the formed optimized product is not the proper one, since the C_{12}-C_{13} is trans both in LXA_4 and LXB_4. It is important to notice that the antarafacial approach is hindered by Leu408. The potential energy barrier for this suprafacial oxygen attack turns out to be 34.1 kcal/mol (this barrier is even bigger, 43.8 kcal/mol, if the water molecule is eliminated), which is too high for the process to be feasible, and the reaction is exoergic by -22.4 kcal/mol. The barrier appears when the distance between the oxygen molecule and C_{14} is around 2.00 Å. Taking everything into

account, we can conclude that the oxygen addition in the case 5(*S*),15(*S*)-diHETE is not possible either to C_6 (no channel leads to C_6 due to the steric hindrance by Ile173, Leu408 and the hydroxyl group at C_5) or to C_{14}.

As for 5(*S*),15(*S*)-diHpETE, the selected oxygen channel is narrower than in the case of 5(*S*),15(*S*)-diHETE, and it becomes more and more tighten as it approaches to $C_{14,}$ so that only the oxygen molecule fits in it. Leu408, Ile414, Phe175, Ile593, and Leu597 limit the diameter of the channel (see Figure 15b and Figure S19). Moreover, the oxygen molecule's addition to C_{14} is now antarafacial. Thus, this approach gives rise to a trans bond between C_{12} and C_{13} which also agrees with the experimental structures of lipoxins. In this case, the oxygen molecule penetrates into the channel practically barrierless until reaching a first energy minimum ($d(C_{14}\text{-}O_2)$ = 2.64 Å), where it must overcome a small potential energy barrier (the corresponding transition state structure appears for a $d(C_{14}\text{-}O_2)$ = 2.03 Å, with a barrier of 3.5 kcal/mol) to reach a second energy minimum ($d(C_{14}\text{-}O_2)$ = 1.51 Å). The process between both energy minima is exoergic by 2.5 kcal/mol. The structures corresponding to these three stationary points are shown in Figures S20 to S22. In order to discuss if this is actually a favorable process, we have combined the umbrella sampling method[32] with the weighted histogram analysis method[33] (WHAM) to calculate the free energy barrier for that addition to C_{14} of 5S,15S-diHpETE. Seven windows and five windows were selected to cover, respectively, the path up to the first minimum and the evolution to the second energy minimum. 0.3 ps of equilibration plus 2 ps of production time were simulated for each window. Measured from the beginning of the path, the approach to the first minimum involves a free energy barrier of 1.4 kcal/mol, and for the second step, 3.1 kcal/mol. These numbers indicate that this addition is a favorable process. All these results prove that the oxygen molecule addition to C_{14} for the case of 5(*S*),15(*S*)-diHpETE is quite easy, leading later to the formation of $LXB_{4.}$

For the sake of completeness, the possibility of the oxygen molecule addition to C_6 for the case of 5(*S*),15(*S*)-diHpETE has also been studied. The procedure has been the same as for the addition to C_{14}, but taken now the distance C_6-O to define the reaction coordinate. However, this process involves a too high potential energy barrier of 34.9 kcal/mol. The oxygen molecule approach is antarafacial, but it is blocked by C_4 of 5(*S*),15(*S*)-diHpETE and the sidechains of Leu408 and Leu 597 (Figure S19). All of them must move away to allow the oxygen molecule to pass towards C_6. Besides, there is an important reorganization of C_6 and C_7 to adjust to the oxygen entrance at C_6. That is the reason why LXA_4 cannot be formed.

Joining together the results of this section, it can be concluded that the oxygen addition is the reaction mechanism's step which explains why 5(*S*),15(*S*)-diHETE is not oxidized while 5(*S*),15(*S*)-diHpETE is oxidized, but just at C_{14}, not at C_6.

3.3.3.3. Rotation of one of the C-C bonds that contains the peroxide moiety in the case of 5(*S*),15(*S*)-diHpETE

As explained in the Introduction, after the C_{10} hydrogen abstraction, the oxygenation mechanism to produce lipoxins involves addition of molecular oxygen followed by a back-hydrogen transfer to the peroxide radical to form the corresponding hydroperoxide. Due to the fact that the oxygen molecule attacks the π nonatetraenyl radical derived from 5(*S*),15(*S*)-diHpETE at C_{14} antarafacially to the Fe atom, a rotation of one of the C-C bonds that contains the peroxide moiety to achieve a suprafacial arrangement is necessary to make feasible the back-hydrogen transfer from the Fe^{II} - OH_2 group of the enzyme. In this section, only this rotation for 5(*S*),15(*S*)-diHpETE is studied since this is the only substrate that can be oxygenated.

The optimized product of the 5(*S*),15(*S*)-diHpETE oxygenation at C_{14} (see Figure S22) was selected as starting point to begin this rotation. The reaction coordinate to reach a suprafacial arrangement of the peroxide radical was defined as a rotation around one of the C-C bonds that contains this group. This movement can be described by the dihedral angle centered on the carbon atoms that define the bond around which the rotation is performed. So, two dihedral angles, $<C_{12}$-C_{13}-**C_{14}**-C_{15} and $<C_{13}$-**C_{14}**-C_{15}-C_{16}, can be considered, since there are two C-C bonds which contain the peroxide radical. In addition, it is possible to define two rotation directions for each dihedral angle, clockwise and counterclockwise (these rotations are defined looking at the substrate from the carboxylate side, see Figures S23 and S24). Thus, there are four possible dihedral angle rotations to reach the suprafacial arrangement. However, visualizing the starting structure, it can be noted that both counterclockwise rotations (see Figure S23) would produce important clashes between the protein and the substrate (especially between the peroxide at C_{14} and Glu357), which would require a big substrate's reorganization to make them possible. For this reason, both counterclockwise rotations can be passed over. On the one hand, the clockwise rotation (see Figure S24) of the dihedral angle $<C_{12}$-C_{13}-**C_{14}**-C_{15} could not reach a complete rotation of the peroxide radical from an antarafacial to a suprafacial arrangement. This result brings out the flexible nature of the substrate. Our calculations along the corresponding reaction coordinate show that the peroxide radical barely can progress to a suprafacial disposal, but, instead, the rest of the atoms of 5(*S*),15(*S*)-diHpETE are the ones that reorganize as this rotation progresses. On the other hand, the clockwise rotation of the dihedral angle $<C_{13}$-**C_{14}**-C_{15}-C_{16} does lead to a suprafacial disposal of the peroxide radical even though the outer oxygen atom of this radical is not directed towards the Fe atom. The potential energy profile for this rotation exhibits a quite smooth curve. The located suprafacial product (see Figure S26) located

from it is found at 64.1° and the corresponding transition state structure (see Figure S25) involves a potential energy barrier of 14.5 kcal/mol, with a reaction energy of 13.3 kcal/mol.

3.3.3.4. Back-hydrogen transfer to the peroxide moiety in the case of 5(S),15(S)-diHpETE

Once the peroxide radical has reached a suprafacial arrangement by a suitable rotation around the dihedral angle <C_{13}-**C_{14}**-C_{15}-C_{16}, more conformational changes are necessary because the orientation of the outer oxygen atom of this peroxide radical is not suited regarding the Fe atom. An additional rotational motion is needed to approach this oxygen atom to one of the hydrogen atoms of the Fe^{II}-OH_2 cofactor. With the aim of both correcting this bad orientation and carrying out the back-hydrogen transfer to the peroxide radical, the reaction coordinate has been defined as the difference between the breaking bond length (O – H of the OH_2 in the cofactor) and the forming bond length (O – H of the final hydroperoxide group).

As starting point for this reaction profile, the QM/MM optimized structure of the minimum energy suprafacial structure at 64.1° for the dihedral angle <C_{13}-**C_{14}**-C_{15}-C_{16} has been selected (Figure S26). This process presents two potential energy barriers. On the one hand, the first barrier corresponds to an important substrate's reorganization and a rotation of the H_2O molecule of the Fe^{II}-OH_2 cofactor. The substrate's reorganization consists of rotations around the C-C bonds, which always maintain the C=C bonds stereochemistry of the final product, and a rotation around the C-O bond of the peroxide radical. As result of all these rotations the outer oxygen atom of the peroxide radical is already quite close to the hydrogen atom of the Fe^{II}-OH_2 cofactor that will be back transferred and both atoms are facing each other. All this process proceeds with a potential

energy barrier of 15.6 kcal/mol and a reaction energy of 8.5 kcal/mol (see Figures S27 and S28). On the other hand, the second barrier corresponds to the back-hydrogen transfer itself. The corresponding located transition state structure (see Figure S29) involves a potential energy barrier of 19.3 kcal/mol and a reaction energy of 1.9 kcal/mol with respect to the energy minimum (Figure S28) located after that first barrier. As result of this process, the peroxide radical is reduced to a hydroperoxide group and the Fe^{III}-OH^- cofactor is regenerated to initiate a new catalytic cycle. Thus, the 5*S*,14*R*,15*S*-trihydroperoxy-6*E*,8*Z*,10*E*,12*E*-eicosatetraenoic acid (5*S*,14*R*,15*S*-triHpETE) is formed (see Figure S30), which has to be finally transformed to LXB_4 by means of a reductase.

4. Conclusions

A deep understanding of the biosynthetic pathways for the specialized pro-resolving lipid mediators, like lipoxins, is required in order to both activate endogenous resolution pathways as novel therapeutic approaches and get efficient exogenous pharmaceutical drugs for the treatment of human diseases that involves serious chronic inflammations, including COVID-19.[34–36] In this paper we have combined molecular dynamics (MD) simulations and quantum mechanics/molecular mechanics (QM/MM) calculations to get a deeper molecular insight on the formation of the inflammatory suppressors lipoxins in the 5(*S*),15(*S*)-diHpETE biosynthetic pathway catalyzed by reticulocyte 15-lipoxygenase-1.

The process begins by means of a quite easy hydrogen abstraction from the C_{10} carbon atom of 5(*S*),15(*S*)-diHpETE by 15-LOX-1. The abstraction barrier is quite lower than in the case of arachidonic acid due to the extended conjugation over the nine carbon atoms (C_6 - C_{14}) of the π nonatetraenyl radical formed. After that, our results do not predict the formation of lipoxins by means of the dehydration mechanism. This result is compatible with the fact that no epoxide has been directly detected as an intermediate in the catalytic

formation of lipoxins from 5(S),15(S)-diHpETE. In fact, in the product of the C_{10} hydrogen abstraction the hydrogen atoms of the Fe^{II} - OH_2 cofactor are oriented towards the hydroperoxide group at C_5, with its oxygen atom placed above the C_9-C_{10} bond. As a consequence, the hydrogen atom to be transferred is too far away from the hydrogen acceptor oxygen atom of the hydroperoxide at C_{15}, what impedes to couple the epoxide formation with the water formation. The hydroperoxide group at C_5 of 5(*S*),15(*S*)-diHpETE forms a hydrogen bond with the terminal Ile663 (in the Fe coordination sphere), which in turn is forming a hydrogen bond with the OH group of the cofactor. This is the key point why the Fe atom and its coordination sphere (including the OH group) keep clearly closer to C_5 and its hydroperoxide than to C_{15} and its hydroperoxide. This way the formation of the 14,15-epoxide is not predicted to be possible. On the other hand, the 5,6-epoxide formation is unattainable because it is hindered by Ile663 which is placed between the Fe^{II} - OH_2 cofactor and the hydroperoxide at C_5.

The formation of lipoxins takes place through the oxygen molecule addition to the π nonatetraenyl radicals derived from 5(*S*),15(*S*)-diHpETE by the C_{10} hydrogen abstraction. The oxygen molecule addition to C_{14} is very easy, leading later to the formation of LXB_4. However, the oxygen molecule addition to C_6 is blocked by C_4 of 5(*S*),15(*S*)-diHpETE and the sidechains of Leu408 and Leu 597. There is also an important reorganization of C_6 and C_7 to adjust to the oxygen entrance at C_6. That is the reason why LXA_4 cannot be formed from 5(*S*),15(*S*)-diHpETE by 15-LOX-1.

Because the oxygen molecule attacks at C_{14} antarafacially to the Fe atom, a rotation of one of the C-C bonds that contains the peroxide moiety to reach a suprafacial arrangement is required to make feasible the back-hydrogen transfer from the Fe^{II} - OH_2 group of 15-LOX-1. Then, the peroxide radical is reduced to a hydroperoxide group. This way the

5*S*,14*R*,15*S*-trihydroperoxy-6*E*,8*Z*,10*E*,12*E*-eicosatetraenoic acid (5*S*,14*R*,15*S*-triHpETE) is formed, which must be finally converted to LXB_4 by means of a reductase. For the sake of comparison, we have also studied the behavior of 5(*S*),15(*S*)-diHETE as substrate. Hydrogen abstraction from C_{10} turns out to be somewhat slower than in the case of 5(*S*),15(*S*)-diHpETE, but again the energy barrier is quite lower than in the case of arachidonic acid. Indeed 5(*S*),15(*S*)-diHETE cannot generate any epoxides. Moreover, the oxygen molecule addition is not possible either to C_6 (no oxygen access channel leading to C_6 exists) or to C_{14} (the antarafacial approach to it is hindered by Leu408). Thus, 15-LOX-1 cannot convert 5(*S*),15(*S*)-diHETE to a lipoxin, in good agreement with the experimental results.[11]

Supporting Information Available: This material is available free of charge at https://pubs.acs.org/...

Details of the Molecular Dynamics simulations and of the QM/MM calculations, and the corresponding References; AMBER parameter files; Representative structures of the second most populated clusters corresponding to the docking of 5(*S*),15(*S*)-diHpETE and 5(*S*),15(*S*)-diHETE; structures of the stationary points; representative oxygen molecule channels corresponding to the main cluster for the case of 5(*S*),15(*S*)-diHETE and for the case of 5(*S*),15(*S*)-diHpETE; definition of the two counterclockwise and the two clockwise C-C rotations considered in the optimized product of the 5(*S*),15(*S*)-diHpETE oxygenation at C_{14}.

Acknowledgements

We thank the Spanish "Ministerio de Ciencia, Innovación y Universidades" for Grant CTQ2017-83745-P. We acknowledge CSUC for computational facilities.

References

(1) Ayoub, S. S. *Fundamentals of Inflammation*; Serhan, C. N., Ward, P. A., Gilroy, D. W., Eds.; Cambridge University Press: Cambridge, **2010**.

(2) Bannenberg, G.; Serhan, C. N. Specialized Pro-Resolving Lipid Mediators in the Inflammatory Response: An Update. *Biochimica et Biophysica Acta - Molecular and Cell Biology of Lipids*. **2010**, *1801* ,1260–1273.

(3) Serhan, C. N. Treating Inflammation and Infection in the 21st Century: New Hints from Decoding Resolution Mediators and Mechanisms. *The Faseb Journal.* **2017**, *31*,1273–1288.

(4) Serhan, C. N.; Hamberg, M.; Samuelsson, B. Trihydroxytetraenes: A Novel Series of Compounds Formed from Arachidonic Acid in Human Leukocytes. *Biochem. Biophys. Res. Commun.* **1984**, *118*, 943–949.

(5) Serhan, C. N.; Hamberg, M.; Samuelsson, B. Lipoxins: Novel Series of Biologically Active Compounds Formed from Arachidonic Acid in Human Leukocytes. *Proc. Natl. Acad. Sci. U. S. A.* **1984**, *81*, 5335–5339.

(6) Catalano, A.; Procopio, A. New Aspects on the Role of Lipoxygenases in Cancer Progression. *Histology and Histopathology*. **2005**, *20*, 969–975.

(7) Dobrian, A. D.; Lieb, D. C.; Cole, B. K.; Taylor-Fishwick, D. A.; Chakrabarti, S. K.; Nadler, J. L. Functional and Pathological Roles of the 12- and 15-Lipoxygenases. *Progress in Lipid Research*. **2011**, *50*, 115–131.

(8) Haeggström, J. Z.; Funk, C. D. Lipoxygenase and Leukotriene Pathways: Biochemistry, Biology, and Roles in Disease. *Chemical Reviews*. **2011**, *111*, 5866–5896.

(9) Joo, Y. C.; Oh, D. K. Lipoxygenases: Potential Starting Biocatalysts for the Synthesis of Signaling Compounds. *Biotechnology Advances*. **2012**, *30*, 1524–1532.

(10) Newcomer, M. E.; Brash, A. R. The Structural Basis for Specificity in Lipoxygenase Catalysis. *Protein Science*. **2015**, *24*, 298–309.

(11) Green, A. R.; Freedman, C.; Tena, J.; Tourdot, B. E.; Liu, B.; Holinstat, M.; Holman, T. R. 5 S,15 S-Dihydroperoxyeicosatetraenoic Acid (5,15-DiHpETE) as a Lipoxin Intermediate: Reactivity and Kinetics with Human Leukocyte 5-Lipoxygenase, Platelet 12-Lipoxygenase, and Reticulocyte 15-Lipoxygenase-1. *Biochemistry* **2018**, *57*, 6726–6734.

(12) Kuhn, H.; Wiesner, R.; Alder, L.; Fitzsimmons, B. J.; Rokach, J.; Brash, A. R. Formation of Lipoxin B by the Pure Reticulocyte Lipoxygenase via Sequential Oxygenation of the Substrate. *Eur. J. Biochem.* **1987**, *169*, 593–601.

(13) Rai, G.; Kenyon, V.; Jadhav, A.; Schultz, L.; Armstrong, M.; Jameson, J. B.; Hoobler, E.; Leister, W.; Simeonov, A.; Holman, T. R.; et al. Discovery of Potent and Selective Inhibitors of Human Reticulocyte 15-Lipoxygenase-1. *J. Med. Chem.* **2010**, *53*, 7392–7404.

(14) Choi, J.; Chon, J. K.; Kim, S.; Shin, W. Conformational Flexibility in Mammalian 15S-lipoxygenase: Reinterpretation of the Crystallographic Data. *Proteins Struct. Funct. Bioinforma.* **2008**, *70*, 1023–1032.

(15) Gordon, J. C.; Myers, J. B.; Folta, T.; Shoja, V.; Heath, L. S.; Onufriev, A. H++: A Server for Estimating PKas and Adding Missing Hydrogens to Macromolecules.

Nucleic Acids Res. **2005**, *33*, W368–W371.

(16) Anandakrishnan, R.; Aguilar, B.; Onufriev, A. V. H++ 3.0: Automating PK Prediction and the Preparation of Biomolecular Structures for Atomistic Molecular Modeling and Simulations. *Nucleic Acids Res.* **2012**, *40*, W537–W541.

(17) Jones, G.; Willett, P.; Glen, R. C.; Leach, A. R.; Taylor, R. Development and Validation of a Genetic Algorithm for Flexible Docking. *J. Mol. Biol.* **1997**, *267*, 727–748.

(18) D.A. Case, I.Y. Ben-Shalom, S.R. Brozell, D.S. Cerutti, T.E. Cheatham, III, V.W.D. Cruzeiro, T.A. Darden, R.E. Duke, D. Ghoreishi, M.K. Gilson, et al. AMBER 2018. University of California: San Francisco 2018.

(19) Sherwood, P.; De Vries, A. H.; Guest, M. F.; Schreckenbach, G.; Catlow, C. R. A.; French, S. A.; Sokol, A. A.; Bromley, S. T.; Thiel, W.; Turner, A. J.; et al. QUASI: A General Purpose Implementation of the QM/MM Approach and Its Application to Problems in Catalysis. *J. Mol. Struct. THEOCHEM* **2003**, *632*, 1–28.

(20) Metz, S.; Kästner, J.; Sokol, A. A.; Keal, T. W.; Sherwood, P. ChemShell-a Modular Software Package for QM/MM Simulations. *Wiley Interdiscip. Rev. Comput. Mol. Sci.* **2014**, *4*, 101–110.

(21) Ahlrichs, R.; Bär, M.; Häser, M.; Horn, H.; Kölmel, C. Electronic Structure Calculations on Workstation Computers: The Program System Turbomole. *Chem. Phys. Lett.* **1989**, *162*, 165–169.

(22) Smith, W.; Forester, T. R. DL-POLY-2.0: A General-Purpose Parallel Molecular Dynamics Simulation Package. *J. Mol. Graph.* **1996**, *14*, 136–141.

(23) Bakowies, D.; Thiel, W. Hybrid Models for Combined Quantum Mechanical and Molecular Mechanical Approaches. *J. Phys. Chem.* **1996**, *100*, 10580–10594.

(24) Senn, H. M.; Thiel, W. QM/MM Methods for Biomolecular Systems. *Angewandte*

Chemie - International Edition. **2009**, *48*, 1198–1229.

(25) De Vries, A. H.; Sherwood, P.; Collins, S. J.; Rigby, A. M.; Rigutto, M.; Kramer, G. J. Zeolite Structure and Reactivity by Combined Quantum-Chemical-Classical Calculations. *J. Phys. Chem. B* **1999**, *103*, 6133–6141.

(26) Chovancova, E.; Pavelka, A.; Benes, P.; Strnad, O.; Brezovsky, J.; Kozlikova, B.; Gora, A.; Sustr, V.; Klvana, M.; Medek, P.; et al. CAVER 3.0: A Tool for the Analysis of Transport Pathways in Dynamic Protein Structures. *PLoS Comput. Biol.* **2012**, *8*, e1002708.

(27) Humphrey, W.; Dalke, A.; Schulten, K. VMD: Visual Molecular Dynamics. *J. Mol. Graph.* **1996**, *14*, 33–38.

(28) Pettersen, E. F.; Goddard, T. D.; Huang, C. C.; Couch, G. S.; Greenblatt, D. M.; Meng, E. C.; Ferrin, T. E. UCSF Chimera - A Visualization System for Exploratory Research and Analysis. *J. Comput. Chem.* **2004**, *25*, 1605–1612.

(29) Saura, P.; Suardíaz, R.; Masgrau, L.; Lluch, J. M.; González-Lafont, À. Unraveling How Enzymes Can Use Bulky Residues to Drive Site-Selective c-h Activation: The Case of Mammalian Lipoxygenases Catalyzing Arachidonic Acid Oxidation. *ACS Catal.* **2014**, *4*, 4351–4363.

(30) Jin, J.; Zheng, Y.; Boeglin, W. E.; Brash, A. R. Biosynthesis, Isolation, and NMR Analysis of Leukotriene A Epoxides: Substrate Chirality as a Determinant of the Cis or Trans Epoxide Confi Guration. *J. Lipid Res.* **2013**, *54*, 754–761.

(31) Smyrniotis, C. J.; Barbour, S. R.; Xia, Z.; Hixon, M. S.; Holman, T. R. ATP Allosterically Activates the Human 5-Lipoxygenase Molecular Mechanism of Arachidonic Acid and 5(S)-Hydroperoxy-6(E),8(Z),11(Z),14(Z)-Eicosatetraenoic Acid. *Biochemistry* **2014**, *53*, 4407–4419.

(32) *Series in Chemical Physics: Free Energy Calculations. Theory and Applications*

in Chemistry and Biology; Chipot, Ch., Pohorille, A., Eds.; Springer: New York, **2007**.

(33) Kumar, S.; Rosenberg, J. M.; Bouzida, D.; Swendsen, R. H.; Kollman, P. A. The Weighted Histogram Analysis Method for Free-energy Calculations on Biomolecules. I. The Method. *J. Comput. Chem.* **1992**, *13*, 1011–1021.

(34) Das, U. N. Can Bioactive Lipids Inactivate Coronavirus (COVID-19)? *Arch. Med. Res.* **2020**, *51*, 282–286.

(35) Freedman, C.; Tran, A.; Tourdot, B. E.; Kalyanaraman, C.; Perry, S.; Holinstat, M.; Jacobson, M. P.; Holman, T. R. Biosynthesis of the Maresin Intermediate, 13S,14S-Epoxy-DHA, by Human 15-Lipoxygenase and 12-Lipoxygenase and Its Regulation through Negative Allosteric Modulators. *Biochemistry* **2020**, *59*, 1832–1844.

(36) Panigrahy, D.; Gilligan, M. M.; Huang, S.; Gartung, A.; Cortés-Puch, I.; Sime, P. J.; Phipps, R. P.; Serhan, C. N.; Hammock, B. D. Inflammation Resolution: A Dual-Pronged Approach to Averting Cytokine Storms in COVID-19? *Cancer and Metastasis Reviews*. **2020**, *39*, 337–340.

Table of Contents graphic